

# On Adaptive Frequency Sampling for Data-driven MOR Applied to Antenna Responses

Lucas Åkerstedt, Darwin Blanco, and B. L. G. Jonsson

**Abstract**—Frequency domain sweeps of array antennas are well-known to be time-intensive, and different surrogate models have been used to improve the performance. Data-driven model order reduction algorithms, such as the Loewner framework and vector fitting, can be integrated with these adaptive error estimates, in an iterative algorithm, to reduce the number of full-wave simulations required to accurately capture the requested frequency behavior of multiport array antennas. In this work, we propose two novel adaptive methods exploiting a block matrix function which is a key part of the Loewner framework generating system approach. The first algorithm leverages an inherent matrix parameter freedom in the block matrix function to identify frequency points with large errors, whereas the second utilizes the condition number of the block matrix function. Both methods effectively provide frequency domain error estimates, which are essential for improved performance. Numerical experiments on multiport array antenna S-parameters demonstrate the effectiveness of our proposed algorithms within the Loewner framework.

**Index Terms**—Adaptive frequency sampling, adaptive interpolation, frequency domain simulations, Loewner framework, frequency sweeps, S-parameters.

## I. INTRODUCTION

**S**IMULATING antenna array responses in the frequency domain is often time-consuming. For example, in Method of Moments (MoM) one needs to calculate the impedance matrix and solve a linear system for each frequency point. The total required time depends on the mesh size, the number of antenna ports, and the frequency band of the problem. Furthermore, the simulation challenges become even larger when out-of-band properties are needed [1].

One method to speed up the process is to determine fewer frequency points in contribution with interpolation [2], [3]. Methods that address the matrix completion time include using the Toeplitz structure [4] and methods to solve the linear system fast include iterative methods [5].

In this work, we limit our attention to rational approximations of complex systems by the use of interpolation. It is well known that antenna systems are not *rational systems* [6]. Rational systems are, however, frequently effective in approximating more complex systems [7]–[9].

There exist many algorithms and methods for rational approximation, e.g. Cauchy interpolation [10], [11], vector fitting [12], [13], and the Loewner framework [14]–[16]. The two latter methods are widely used in the area of Model Order

Reduction (MOR), and they are categorized as *non-intrusive* (or *data-driven*) MOR methods [17]. Non-intrusive methods use only the input and output data of a system, and not any prior physical knowledge of a system [18]. In this paper, the two data-driven MOR methods, the Loewner framework and vector fitting, are used and compared.

Comparisons between the Loewner framework and vector fitting have been conducted in [17], [19]–[21]. These papers compare the MOR methods on various frequency responses. Interestingly, there are no comparisons between the methods for antenna frequency responses that we have found. The use of vector fitting and Loewner matrix-based interpolation in an antenna context has, however, been carried out before in [22], [23], and in [24]–[26], respectively. One of the contributions of this paper is a comparison of the Loewner framework and vector fitting, when specifically applied to array antenna responses.

Prior works on *adaptive* frequency sampling algorithms for non-intrusive MOR include the greedy algorithm by Pradovera [27], the heuristic scheme by Vuillemin and Poussot-Vassal [28], and the greedy algorithm by Cherifi *et al.*, [29]. These algorithms aim to select as few frequency samples as possible while still obtaining an accurate rational approximation.

The main contribution of this paper is the comparison of the adaptive frequency sampling algorithms from [27] and [28] with two novel adaptive frequency sampling algorithms based on the *generating system*-approach from [21]. These adaptive methods are tested on antenna array responses in conjunction with the Loewner Framework and vector fitting. In addition, these adaptive methods are also compared with predetermined frequency distributions. From the comparison, the two novel frequency sampling algorithms yield the best performance in terms of accuracy as a function of the number of interpolation points used.

This paper is organized as follows. The theory of scalar vector fitting and the Loewner framework is shown in Section II. Section III introduces the theory of the adaptive sampling algorithms tested in this paper. In Section IV, the adaptive frequency sampling algorithms are tested on various antenna responses. Lastly, Section V concludes the paper.

## II. THEORY

### A. Vector Fitting

Vector fitting is well described in [12], [18]. We repeat the main steps in the scalar case for completeness. Let  $s \in \mathbb{C}$  be the complex Laplace variable such that  $s = j\omega$ , where  $\omega \in \mathbb{R}$

Lucas Åkerstedt and B. L. G. Jonsson are with KTH Royal Institute of Technology, EECS, 100 44 Stockholm, Sweden (e-mail: lucasak@kth.se).

Darwin blanco is with Standards & Technology Ericsson AB, Stockholm, Sweden.

is the angular frequency. Vector fitting approximates the scalar function  $S(s)$  as a rational function  $h(s)$ ,

$$h(s) = \sum_{n=1}^N \frac{r_n}{s - a_n} + d + se, \quad (1)$$

where  $r_n \in \mathbb{C}$  are the residues,  $a_n \in \mathbb{C}$  are the poles, and  $d, e \in \mathbb{C}$  are the asymptotic expansion coefficients. Solving for the coefficients in (1) is a non-linear problem that is linearized and solved iteratively by first creating the augmented problem

$$\begin{cases} \sigma(s)h(s) \approx \sum_{n=1}^N \frac{r_n}{s - \tilde{a}_n} + d + se \\ \sigma(s) \approx \sum_{n=1}^N \frac{\tilde{r}_n}{s - \tilde{a}_n} + 1 \end{cases}, \quad (2)$$

where  $\tilde{a}_n$  are the starting poles and are set according to a heuristic scheme. Multiplying  $\sigma(s)$  from (2) with  $h(s)$  and rearranging yields

$$\sum_{n=1}^N \frac{r_n}{s - \tilde{a}_n} + d + se - h(s) \sum_{n=1}^N \frac{\tilde{r}_n}{s - \tilde{a}_n} \approx h(s). \quad (3)$$

Given  $\{s_i, S(s_i)\}_{i=1}^{N_s}$  and  $h(s_i) = S(s_i)$ , (3) yields a linear system that is solved in the least square sense. Solving the linear system yields the approximative solution to the unknown coefficients,  $r_n, \tilde{r}_n, d, e$ . Given  $\{\tilde{r}_n\}$  a new set of poles  $\{\tilde{a}_n\}$  are obtained by solving the eigenvalue problem

$$\{\tilde{a}_n\} = \text{eig}(\tilde{\mathbf{A}} - \tilde{\mathbf{b}} \cdot \tilde{\mathbf{r}}). \quad (4)$$

Here,  $\tilde{\mathbf{A}} = \text{diag}(\tilde{a}_1, \dots, \tilde{a}_N)$ ,  $\tilde{\mathbf{b}} = [1, \dots, 1]^T$ , and  $\tilde{\mathbf{r}} = [\tilde{r}_1, \dots, \tilde{r}_N]^T$ . The procedure (3) - (4) is repeated for a number of iterations. The final set of poles is inserted into (1), which leaves a linear problem, solved in the least square sense to obtain the final set of residues  $\{r_n\}$  and the asymptotic coefficients  $d$  and  $e$ . For a generalization to the matrix case, see [18].

### B. The Block Loewner Framework

With the block Loewner framework [14], [21], the transfer function matrix at each sample is used as data. Given the discrete data set  $P = \{s_i, \mathbf{S}(s_i)\}_{i=1}^{N_s}$ , where  $\mathbf{S}(s_i) \in \mathbb{C}^{p \times m}$ , the set is partitioned into two disjoint sets

$$\begin{cases} P_c = \{(\lambda_i, \mathbf{w}_i) : i = 1, \dots, k\} \\ P_r = \{(\mu_j, \mathbf{v}_j) : j = 1, \dots, q\} \end{cases}, \quad (5)$$

where

$$\left. \begin{aligned} \lambda_i = s_i, \quad \mathbf{w}_i = \mathbf{S}(\lambda_i), \quad i = 1, \dots, k \\ \mu_j = s_{k+j}, \quad \mathbf{v}_j = \mathbf{S}(\mu_j), \quad j = 1, \dots, q \end{aligned} \right\}, \quad k + q = N_s. \quad (6)$$

In this paper, we use *alternate splitting* [16] for partitioning the set  $P$  into  $P_c$  and  $P_r$ . With alternate splitting, the frequencies  $s_i$  are sorted according to their angular frequency  $\omega_i$ . Then, every other frequency is said to belong to  $P_c$ . The remaining frequencies are said to belong to  $P_r$ .

From the two data sets  $P_c$  and  $P_r$ , the left and right data (or more precisely, row and column data) are constructed as follows:

$$\left. \begin{aligned} \mathbf{A} &= \text{diag}(\lambda_1, \dots, \lambda_k) \otimes \mathbb{I}_m \in \mathbb{C}^{(mk) \times (mk)} \\ \mathbf{R} &= [\mathbb{I}_m, \dots, \mathbb{I}_m] \in \mathbb{C}^{m \times (mk)} \\ \mathbf{W} &= [\mathbf{w}_1, \dots, \mathbf{w}_k] \in \mathbb{C}^{p \times (mk)} \end{aligned} \right\}, \quad (7)$$

where  $\mathbb{I}_m$  is the  $m \times m$  identity matrix, and  $\otimes$  indicates the Kronecker product.

From the data set  $P_r$ , the left data (row data) is constructed

$$\left. \begin{aligned} \mathbf{M} &= \text{diag}(\mu_1, \dots, \mu_q) \otimes \mathbb{I}_p \in \mathbb{C}^{(pq) \times (pq)} \\ \mathbf{L} &= [\mathbb{I}_p, \dots, \mathbb{I}_p]^T \in \mathbb{C}^{(pq) \times p} \\ \mathbf{V} &= [\mathbf{v}_1^T, \dots, \mathbf{v}_q^T]^T \in \mathbb{C}^{(pq) \times m} \end{aligned} \right\}. \quad (8)$$

For other approaches to constructing the left and right data, e.g. *tangential* interpolation, see [14], [15], [21].

From the left and right data, the *block Loewner matrix* is constructed

$$\mathbb{L} = \begin{bmatrix} \frac{\mathbf{v}_1 - \mathbf{w}_1}{\mu_1 - \lambda_1} & \dots & \frac{\mathbf{v}_1 - \mathbf{w}_k}{\mu_1 - \lambda_k} \\ \vdots & \ddots & \vdots \\ \frac{\mathbf{v}_q - \mathbf{w}_1}{\mu_q - \lambda_1} & \dots & \frac{\mathbf{v}_q - \mathbf{w}_k}{\mu_q - \lambda_k} \end{bmatrix} \in \mathbb{C}^{(pq) \times (mk)}. \quad (9)$$

Within the Loewner framework, there exist at least three approaches for constructing an interpolant  $\mathbf{H}(s)$ , such that  $\mathbf{H}(s) \approx \mathbf{S}(s)$ . For the first approach [15, Sec 4], the interpolant  $\mathbf{H}(s)$  is constructed using the state space representation

$$\mathbf{H}(s) = \mathbf{C}(s\mathbb{L} - \mathbf{A})^{-1}\mathbf{B} + \mathbf{D}, \quad (10)$$

where the state space matrices  $\mathbf{A}, \mathbf{B}, \mathbf{C}, \mathbf{D}$  are given by

$$\left( \begin{array}{c|c} \mathbf{A} & \mathbf{B} \\ \mathbf{C} & \mathbf{D} \end{array} \right) = \left( \begin{array}{c|c} \mathbf{A} + \mathbb{L}^\#(\mathbf{V} - \mathbf{LD}) & \mathbb{L}^\#(\mathbf{V} - \mathbf{LD}) \\ \hline -(\mathbf{W} - \mathbf{DR}) & \mathbf{D} \end{array} \right), \quad (11)$$

where  $\mathbf{D}$  is arbitrary, and  $\mathbb{L}^\#$  is the right inverse of  $\mathbb{L}$  (and can be calculated by, e.g. the Penrose-Moore inverse).

The second method of constructing the interpolant is called the *generating system* approach [14], [21]. Here, the block matrix function  $\Theta(s)$ , or its inverse  $\bar{\Theta}(s)$ , is constructed to generate the interpolant with

$$\begin{aligned} \mathbf{H}(s) &= [\Theta_{11}(s)\mathbf{G}_1(s) - \Theta_{12}(s)\mathbf{G}_2(s)] \\ &\quad [-\Theta_{21}(s)\mathbf{G}_1(s) + \Theta_{22}(s)\mathbf{G}_2(s)]^{-1}, \end{aligned} \quad (12)$$

or

$$\begin{aligned} \mathbf{H}(s) &= [\mathbf{G}_1(s)\bar{\Theta}_{11}(s) + \mathbf{G}_2(s)\bar{\Theta}_{21}(s)] \\ &\quad [\mathbf{G}_1(s)\bar{\Theta}_{12}(s) + \mathbf{G}_2(s)\bar{\Theta}_{22}(s)]^{-1}, \end{aligned} \quad (13)$$

where  $\mathbf{G}_1(s)$  and  $\mathbf{G}_2(s)$  are arbitrary polynomial matrices [14]. If  $k = q$ , and  $\mathbb{L}$  is invertible, the block matrices  $\Theta(s) \in \mathbb{C}^{(p+m) \times (p+m)}$  and  $\bar{\Theta}(s) \in \mathbb{C}^{(p+m) \times (p+m)}$  are defined as [14], [21]

$$\begin{aligned} \Theta(s) &= \begin{bmatrix} \mathbb{I}_p & 0 \\ 0 & \mathbb{I}_m \end{bmatrix} + \begin{bmatrix} \mathbf{W} \\ -\mathbf{R} \end{bmatrix} (s\mathbb{L} - \mathbb{L}\mathbf{A})^{-1} [\mathbf{L} \quad \mathbf{V}] \\ &= \begin{bmatrix} \Theta_{11}(s) & \Theta_{12}(s) \\ \Theta_{21}(s) & \Theta_{22}(s) \end{bmatrix}, \end{aligned} \quad (14)$$

and

$$\begin{aligned} \bar{\Theta}(s) &= \begin{bmatrix} \mathbb{I}_p & 0 \\ 0 & \mathbb{I}_m \end{bmatrix} + \begin{bmatrix} -\mathbf{W} \\ \mathbf{R} \end{bmatrix} (s\mathbb{L} - \mathbb{M}\mathbf{L})^{-1} [\mathbf{L} \quad \mathbf{V}] \\ &= \begin{bmatrix} \bar{\Theta}_{11}(s) & \bar{\Theta}_{12}(s) \\ \bar{\Theta}_{21}(s) & \bar{\Theta}_{22}(s) \end{bmatrix}. \end{aligned} \quad (15)$$

The third approach is the barycentric interpolation representation [14]

$$\mathbf{H}(s) = \frac{\sum_{i=1}^k \frac{b_i \mathbf{w}_i}{s - \lambda_i}}{\sum_{i=1}^k \frac{b_i}{s - \lambda_i}}, \quad (16)$$

where  $b_i$  are the barycentric coefficients. The barycentric coefficients  $b_i$  are obtained by solving the optimization problem [27]

$$\begin{aligned} \text{minimize} \quad & \sum_{j=1}^q \left\| \sum_{i=1}^k b_i \frac{\mathbf{v}_j - \mathbf{w}_i}{\mu_j - \lambda_i} \right\|_F^2 \\ \text{subject to} \quad & \sum_{i=1}^k |b_i|^2 = 1, \end{aligned} \quad (17)$$

where  $\|\cdot\|_F$  is the Frobenius norm.

### III. FREQUENCY SAMPLING ALGORITHMS

Frequency domain simulations of antennas yield the frequency response calculated at a given discrete set of frequencies. The duration for calculating the frequency response for one frequency point is often quite high for arrays. It is, therefore, desirable to keep the number of frequency points low while still having enough frequency points for the interpolation to accurately resemble the frequency response. Choosing these frequency points in the given frequency band is in this work denoted as *frequency sampling*, [2], [27].

Frequency points may either be sampled in an adaptive or predetermined manner. Predetermined frequency sampling means that a set of frequency points is chosen prior to any frequency domain calculations.

In adaptive frequency sampling, an initial set of frequency samples is iteratively enriched based on an error estimation over a desired frequency band. First, the error estimation is carried out using the available sample points. Then, the frequency response of the sample point estimated to yield the largest error is determined and added to the available samples. The procedure then continues iteratively until it has reached a maximum number of iterations, or that it estimates that a given error tolerance has been reached. Some error estimation methods utilize properties of the interpolation method, whereas some methods only utilize the data of the interpolants. A general description of the adaptive frequency sampling algorithms presented here is displayed in Algorithm 1.

The number of frequency points in the initial set varies. In [30], a sparse uniformly sampled set is used, whereas in [27], only one to two frequency points are used in the initial set. In this work, we use only two frequency points in the initial set: the lower and upper-frequency limit of the band of interest.

Throughout this paper, we denote the number of samples used for interpolation or curve fitting with  $N_s$ . When the interpolants are *constructed*, they are constructed on a fine grid in the frequency band of interest. This fine grid consists of  $M_s$  equidistantly spaced frequency samples in the frequency band of interest,  $[f_{\min}, f_{\max}]$ . Here, we denote these fine sampled discrete frequencies with  $s'_\ell$ , whereas the samples chosen in an adaptive or predetermined manner are denoted with  $s_i$ . Typically, the chosen samples form a subset of the

fine sampled discrete frequencies in the band of interest, i.e.,  $\{s_i\}_{i=1}^{N_s} \subseteq \{s'_\ell\}_{\ell=1}^{M_s}$ ,  $N_s \leq M_s$ .

---

#### Algorithm 1 General adaptive frequency sampling algorithm

---

**Input:** Initial set of  $N$  samples  $\{s_i, \mathbf{S}(s_i)\}_{i=1}^N$

Number of iterations:  $N_I$

Number of discrete frequency points for interpolant construction:  $M_s$

Band of interest:  $f_{\min}, f_{\max}$

**Output:**  $\mathbf{H}(s'_\ell)$

- 1: Set of samples  $\mathcal{S} = \{s_i, \mathbf{S}(s_i)\}_{i=1}^N$
  - 2: Frequencies for interpolant construction  $\{s'_\ell\}_{\ell=1}^{M_s} = 2\pi j \text{ linspace}(f_{\min}, f_{\max}, M_s)$
  - 3: **for**  $n = 0, \dots, N_I - 1$  **do**
  - 4: Construct interpolant  $\mathbf{H}(s'_\ell)$  with the  $N + n$  samples available, for  $\ell = 1, \dots, M_s$
  - 5: Choose next frequency point  $s_{N+n+1}$ , from analyzing  $\mathbf{H}(s'_\ell)$  (or other interpolation specific properties)
  - 6: Calculate  $\mathbf{S}(s_{N+n+1})$
  - 7: Add sample:  $\mathcal{S} \leftarrow \mathcal{S} \cup \{s_{N+n+1}, \mathbf{S}(s_{N+n+1})\}$
  - 8: **end for**
  - 9: **return**  $\mathbf{H}(s'_\ell)$
- 

For predetermined frequency distributions, any arbitrary distribution of frequency points may be used as long as the choice of points is made before any interpolation is carried out. In this work, we use equidistant and Chebyshev-based distributions. Chebyshev-based distributions are here obtained by the  $x$ -coordinate of  $N_s$  equidistantly spaced (with respect to the arc length) points on the upper half of the circumference of an ellipse, as Fig. 1 suggests. Here, a distribution named *Cheb 0.5* corresponds to a Chebyshev-based distribution obtained with an ellipse with a  $y$ -direction radius of 0.5 and a  $x$ -direction radius of 1.

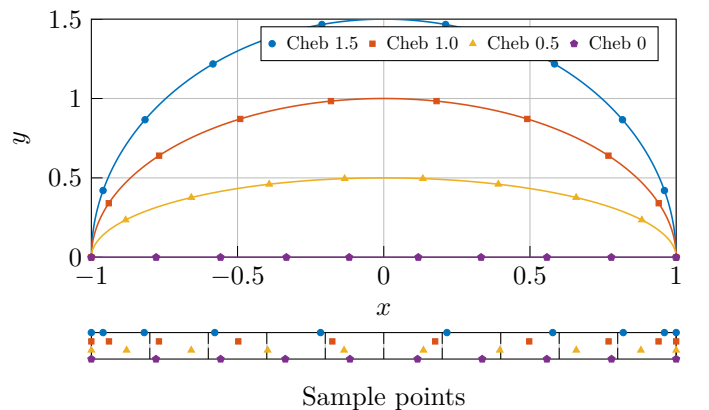


Fig. 1. A visualization of how the Chebyshev-based distributions are calculated.

Each of the proposed methods below, see Section III-B - III-E, utilize different methods to predict the largest error. To compare and quantize the performance of these methods, an error between the constructed interpolant and the true data is calculated. In this paper, all interpolation and sampling meth-

ods are evaluated by the Root Mean Square Error (RMSE), similarly to [17],

$$\text{RMSE} = \left( \frac{1}{M_s} \sum_{\ell=1}^{M_s} \|\mathbf{S}(s'_\ell) - \mathbf{H}(s'_\ell)\|_F^2 \right)^{\frac{1}{2}}, \quad (18)$$

where  $\mathbf{S}(s'_\ell)$  is the testing data, and  $\mathbf{H}(s'_\ell)$  is the constructed interpolant. Throughout Section IV, the testing data consists of scattering parameters calculated for a discrete set of frequencies,  $s'_1, \dots, s'_{M_s}$ , obtained using commercial full-wave simulation software or an in-house MoM solver. Therefore, the interpolants are constructed for the same set of discrete frequencies,  $s'_1, \dots, s'_{M_s}$ , to relieve the use of (18).

In Section IV we also display the relative error between the testing data and the interpolants, as a function of frequency. Here, we consider the Frobenius norm of the element-wise relative error,  $E_{\text{rel}}$ ,

$$E_{\text{rel}}(s'_\ell) = \|\mathbf{E}(s'_\ell)\|_F, \quad E_{ij}(s'_\ell) = \frac{\mathbf{H}_{ij}(s'_\ell) - \mathbf{S}_{ij}(s'_\ell)}{\mathbf{S}_{ij}(s'_\ell) + \delta}, \quad (19)$$

where  $\delta = 10^{-15}$ .

#### A. Double-sided Sampling

The transfer function  $\mathbf{S}(s)$  of an LTI system is *Positive Real* (the admittance or impedance representation) or *Bounded Real* if and only if the LTI system is passive [18, Th 2.1]. Both a positive real and a bounded real transfer function  $\mathbf{S}(s)$  fulfills

$$\mathbf{S}(s)^* = \mathbf{S}(s^*). \quad (20)$$

Given  $N_s$  discrete samples on the imaginary axis,  $\{j\omega_i, \mathbf{S}(j\omega_i)\}_{i=1}^{N_s}$ , of a passive LTI system, the passivity may be exploited to obtain additional  $N_s$  samples. First, consider the sampled set  $\{j\omega_i, \mathbf{S}(j\omega_i)\}_{i=1}^{N_s}$ . Using (20), with the already sampled set, we obtain the set  $\{-j\omega_i, \mathbf{S}(j\omega_i)^*\}_{i=1}^{N_s}$ . This procedure leaves us with the double amount of samples and is here denoted as *double-sided sampling*. In this work, we use double-sided sampling unless stated otherwise.

#### B. Vuillemin Adaptive Frequency Sampling

The adaptive frequency sampling algorithm described in [28] is a heuristic scheme that samples the next frequency point according to the strongest dynamic of the current interpolant. This method identifies the dynamics by finding the peaks and valleys of the current interpolant. In [28], the method is used together with the Loewner framework.

Considering the general description of adaptive frequency sampling in Algorithm 1, the method in [28] specifies line 4, i.e., the analysis of the interpolant (or the properties of the interpolant) to decide the next point to sample. From the current interpolant,  $\mathbf{H}(s'_\ell)$ , a scalar function is defined

$$f(\omega_\ell) = \|\mathbf{H}(j\omega_\ell)\|_2, \quad (21)$$

where  $\|\cdot\|_2$  is the  $\ell^2$ -norm. The discrete frequency corresponding to the largest or lowest value of  $f(\omega_\ell)$  is then chosen as the candidate point. If there are no peaks nor valleys, the frequency point corresponding to the largest or smallest discrete derivative of  $f(\omega_\ell)$  is selected as the candidate point.

#### C. Pradovera Adaptive Frequency Sampling

Another adaptive sampling algorithm to investigate is the greedy sampling algorithm described by Pradovera in [27]. In [27], an adaptive sampling algorithm is constructed based on the barycentric interpolant representation (see (16)) for the Loewner framework. Pradovera shows that the *relative residual norm*  $\rho(s)$  of the approximation  $\mathbf{H}(s)$  satisfies [27, eq. (10)]

$$\rho(s) = \gamma \left| \sum_{i=1}^k \frac{b_i}{s - \lambda_i} \right|^{-1}, \quad (22)$$

where  $\gamma$  is a frequency-independent constant. Subsequently, the next frequency point is sampled to minimize the magnitude of the norm of the sum in (22). A frequency sampling rule is thus obtained:

$$s_{N_s+1} = \arg \min_s \left| \sum_{i=1}^k \frac{b_i}{s - \lambda_i} \right|. \quad (23)$$

In [27], double sided sampling is used such that  $P_c = \{s_i, \mathbf{S}(s_i)\}_{i=1}^{N_s}$ ,  $P_r = \{s_i^*, [\mathbf{S}(s_i)]^*\}_{i=1}^{N_s}$ .

#### D. Loewner Generating System Based Adaptive Sampling I

Here, we propose the first of our two novel adaptive sampling methods. In [21], an adaptive sampling scheme based on the Loewner generating system approach is described. The method from [21] is employed in a context where a large number of samples are already available, e.g., measured S-parameters. There, the goal is to add a number of (already available) samples in each iteration to be used with the Loewner framework to create a reduced order model.

Recall that in this paper, no samples are available in advance. The choice of the next frequency point to sample is driven by the already sampled frequency points. Similarly to [21], we may, however, use the generating system approach to create an adaptive sampling scheme. The underlying philosophy is as follows:

$N$  interpolants are constructed using the generating function  $\Theta(s)$  (or  $\bar{\Theta}(s)$ , see (14) and (15)) together with a set of different arbitrary matrices  $\mathbf{G}_1^{(\tau)}$  and  $\mathbf{G}_2^{(\tau)}$ ,  $\tau = 1, 2, \dots, N$ . An interpolant constructed from the matrices  $\mathbf{G}_1^{(\tau)}$  and  $\mathbf{G}_2^{(\tau)}$  is in this paper denoted by  $\mathbf{H}^{(\tau)}(s'_\ell)$ . The discrete frequency point for which the interpolants  $\mathbf{H}^{(1, \dots, N)}(s'_\ell)$  differ the most is then selected as the next frequency point to sample. The difference among the interpolants can be calculated in a number of ways. In this paper, the element-wise relative difference is calculated, i.e.,

$$s_{N_s+1} = \arg \max_{\ell, i, j, \tau, \nu} \left| \frac{\mathbf{H}_{ij}^{(\tau)}(s'_\ell) - \mathbf{H}_{ij}^{(\nu)}(s'_\ell)}{\mathbf{H}_{ij}^{(\tau)}(s'_\ell)} \right|. \quad (24)$$

It is, however, possible to perform other sorts of difference calculations, e.g., absolute difference.

The Theta I method relies on the block matrix function  $\Theta(s)$  (or  $\bar{\Theta}(s)$ ), which is only defined for when  $k = q$  and when  $\mathbb{L}$  is invertible. As a consequence, the method must be fed an even number of square matrix samples  $\{s_i, \mathbf{S}(s_i)\}_{i=1}^{N_s}$  unless we modify the calculation of the block matrix  $\Theta(s)$ .

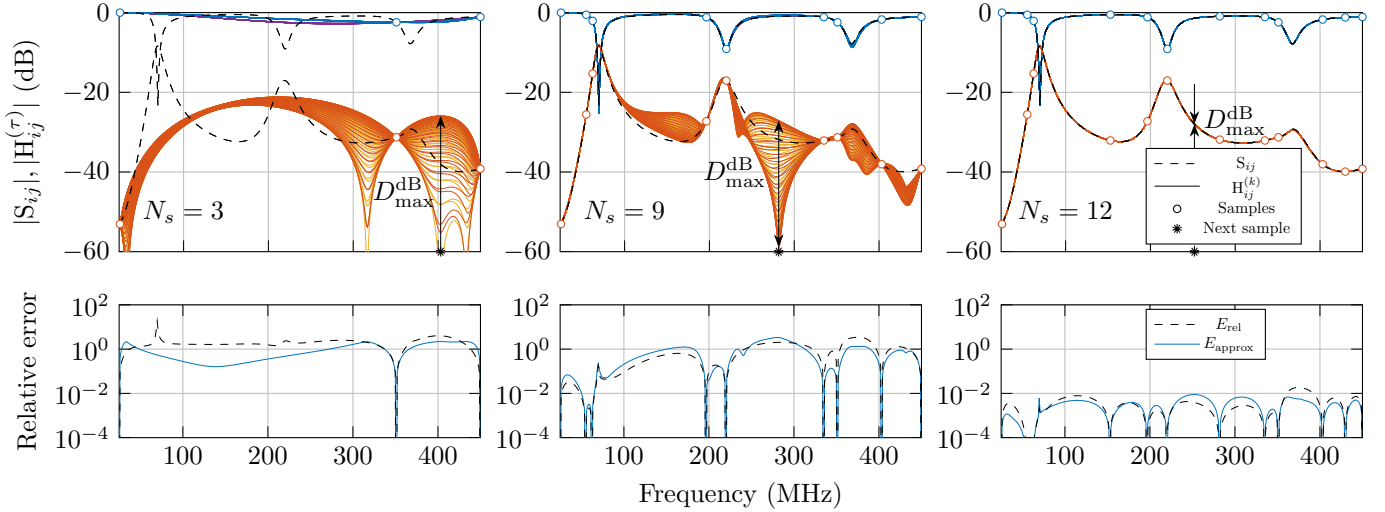


Fig. 2. The 40 interpolants constructed using (12) with the unitary matrices  $\mathbf{G}_1^{(\tau)}$  and  $\mathbf{G}_2^{(\tau)}$ ,  $\tau = 1, \dots, 40$ , for 3, 9, and 12 available samples. The largest relative deviation is highlighted with  $D_{\max}^{\text{dB}}$ , which decides the next frequency point to sample. In the lower plots, the corresponding relative error (19) and the estimated relative error using (25), are displayed.

Here, we propose three ways of managing an odd number of samples. Either use a pseudo-inverse for the calculation of  $(s_{\ell}\mathbb{L} - \mathbb{L}\mathbf{A})^{-1}$ , or Split the  $N_s$  ( $N_s$  being odd) available samples into two groups such that the first group consists of samples  $1, 2, \dots, N_s - 1$ , and the second group consists of samples  $2, 3, \dots, N_s$ . The calculation in (24) is then performed on the two groups separately, which yields us two candidate points. Of the two candidate points, the one corresponding to the largest difference among the corresponding interpolants is chosen. Lastly, the principle of double-sided sampling may be used to always have  $2N_s$  samples available. This solution, however, limits us to passive LTI systems only.

With our proposed method, we may *approximate* the relative error  $E_{\text{rel}}$  by calculating the maximum relative difference among the interpolants:

$$E_{\text{approx}}(s'_{\ell}) = \|\tilde{\mathbf{E}}(s'_{\ell})\|_F, \quad \tilde{\mathbf{E}}_{ij}(s'_{\ell}) = \max_{\tau, \nu} \frac{1}{p} \left| \frac{H_{ij}^{(\tau)}(s'_{\ell}) - H_{ij}^{(\nu)}(s'_{\ell})}{H_{ij}^{(\tau)}(s'_{\ell}) + \delta} \right|. \quad (25)$$

In Fig. 2, we display an example of how the adaptive method is used to interpolate a given antenna response. Here, we interpolate scattering data originating from two 2 m long dipole antennas situated 1 m apart, operating in the frequency band 25 MHz to 450 MHz, with  $50 \Omega$  port impedances. For demonstrative purposes, we have chosen our set of matrices  $\mathbf{G}_1^{(\tau)}$ , and  $\mathbf{G}_2^{(\tau)}$  as unitary  $2 \times 2$  matrices on the form

$$\mathbf{G}_1^{(\tau)} = \begin{bmatrix} w & z \\ -z^* e^{j\theta_{\tau}} & w^* e^{j\theta_{\tau}} \end{bmatrix}, \quad \mathbf{G}_2^{(\tau)} = \begin{bmatrix} x & y \\ -y^* e^{j\theta_{\tau}} & x^* e^{j\theta_{\tau}} \end{bmatrix},$$

$$x = \frac{1}{\sqrt{2}} e^{j\varphi_1}, \quad y = \frac{1}{\sqrt{2}} e^{j\varphi_2}, \quad z = \frac{1}{\sqrt{2}} e^{j\varphi_3}, \quad w = \frac{1}{\sqrt{2}} e^{j\varphi_4}$$

where  $\varphi_1 = 1.1051$ ,  $\varphi_2 = -1.7482$ ,  $\varphi_3 = 2.9750$ ,  $\varphi_4 = 0.9596$ ,  $\theta_{\tau}$  are linearly spaced in the interval  $[0, 2\pi]$ , and  $\tau = 1, 2, \dots, 40$ . Notice how the variation among the 40 interpolants displayed in Fig. 2, for  $N_s = 3, 9, 12$ , decreases as the number of available samples increases.

When the method proposed here is used in the benchmarking cases of Section IV, 6 randomly generated matrices of appropriate size are used (3  $\mathbf{G}_1$  matrices and 3  $\mathbf{G}_2$  matrices). This method has been tested on 6 and 90 randomly generated matrices, with no observed significant change in performance observed across the tests. Hence, for the practical implementation, 6 matrices are generated in MATLAB, with  $2 * \text{rand}(p, m) - 1$ , where  $p$  and  $m$  is the number of rows and columns of the interpolated frequency response.

### E. Loewner Generating System Based Adaptive Sampling II

The here presented method uses the condition number of the block matrix function  $\Theta(s)$  (or  $\bar{\Theta}(s)$ ) as a function of discrete frequency to sample the next frequency point.

The frequency-dependent condition number with respect to the  $\ell^2$ -norm is calculated as,

$$\kappa(\Theta, s'_{\ell}) = \|\Theta(s'_{\ell})\|_2 \|\Theta(s'_{\ell})^{-1}\|_2 = \|\Theta(s'_{\ell})\|_2 \|\bar{\Theta}(s'_{\ell})\|_2. \quad (26)$$

With the condition number as a function of discrete frequency,  $\kappa(\Theta, s'_{\ell})$ , we sample next frequency point according to the lowest corresponding condition number, i.e.,

$$s_{N_s+1} = \arg \min_{s'_{\ell}} \kappa(\Theta, s'_{\ell}). \quad (27)$$

To efficiently calculate  $\Theta(s'_{\ell})$  and  $\bar{\Theta}(s'_{\ell})$ , consider the identities.

$$(s'_{\ell}\mathbb{L} - \mathbb{L}\mathbf{A})^{-1} = (s'_{\ell}\mathbb{I} - \mathbf{A})^{-1}\mathbb{L}^{-1},$$

and

$$(s'_{\ell}\mathbb{L} - \mathbf{M}\mathbb{L})^{-1} = \mathbb{L}^{-1}(s'_{\ell}\mathbb{I} - \mathbf{M})^{-1},$$

where  $\mathbf{A}$  and  $\mathbf{M}$  are diagonal matrices, given in (7) and (8), respectively, for points such that  $\mathbb{L}$  is invertible.

#### IV. NUMERICAL EXAMPLES

In this section, we apply vector fitting and the Loewner framework to antenna frequency responses using both predetermined and adaptive frequency sampling algorithms. Here, the goal is to find the smallest number of frequency samples necessary to reach a certain RMSE tolerance.

When we use the Loewner framework, the interpolants are on the form of (10), with state variables calculated from (11), with  $\mathbf{D} = 0$ .

Due to the Theta I algorithm's dependence on a set of random matrices, the method is tested 30 times (each time with a new set of random matrices, in (12)) in every benchmark case. In each benchmarking graph, the RMSE span of the method is highlighted with the yellow shaded area. The median of the 30 RMSE curves is highlighted with a solid yellow curve.

In each antenna benchmarking case, 30 predetermined frequency distributions are tested using the Loewner framework and vector fitting. These 30 distributions are *Cheb*  $c$ , where  $c$  is linearly spaced in the interval  $[0, 2]$ . For every number of frequency points used, we only display the smallest RMSE reached of all the 30 distributions tested for the Loewner framework and vector fitting, respectively. In the figures, the envelope of minimum RMSE reached by the distributions using the Loewner framework is denoted *Min dist. L*, and the corresponding minimum using vector fitting is denoted *Min dist. vf*. These results provide an ideal 'best case' reference against which the adaptive methods are compared. While it is not quite a reachable predetermined frequency distribution, it gives a lower bound of all the Chebyshev-based distributions. As we will see, it gives a good goal for the adaptive methods.

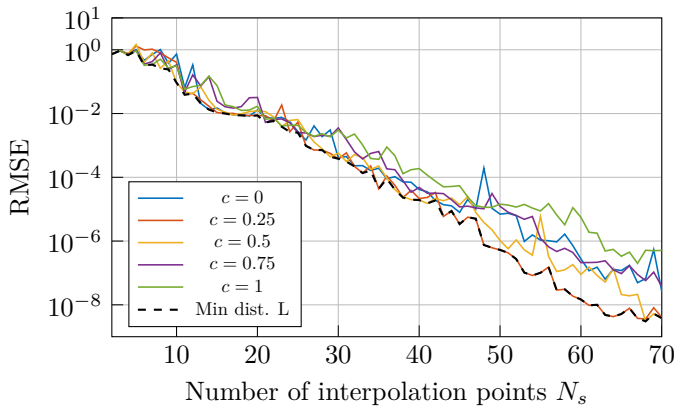


Fig. 3. The RMSE obtained by using the Loewner framework with 5 predetermined frequency sampling distributions, *Cheb*  $c \in [0, 0.25, 0.5, 0.75, 1]$ , that use 2 to 70 interpolation points, for the  $1 \times 4$  bowtie array case. The minimum of the RMSE for each number of interpolation points used is highlighted with the dashed line (*Min dist. L*).

To further clarify and demonstrate the purpose of the envelope of the minimum RMSE using the predetermined frequency distributions, consider a  $4 \times 1$  bowtie array, see inset in Fig. 4. The frequency response  $\mathbf{S}(s'_\ell)$  of the  $4 \times 1$  bowtie array is calculated using with an in-house MoM solver for 400 samples ( $M_s = 400$ ) in the range 1 GHz to 10 GHz. The frequency response  $\mathbf{S}(s'_\ell)$  is then interpolated

using the Loewner framework. The interpolation points are chosen according to the five Chebyshev-based distributions *Cheb*  $c$ ,  $c \in [0, 0.25, 0.5, 0.75, 1]$ . The number of interpolation points  $N_s$  allowed in the distributions, varies from 2 to 70. The resulting RMSE can be seen in Fig. 3, where the envelope of minimum RMSE is highlighted with the dashed line.

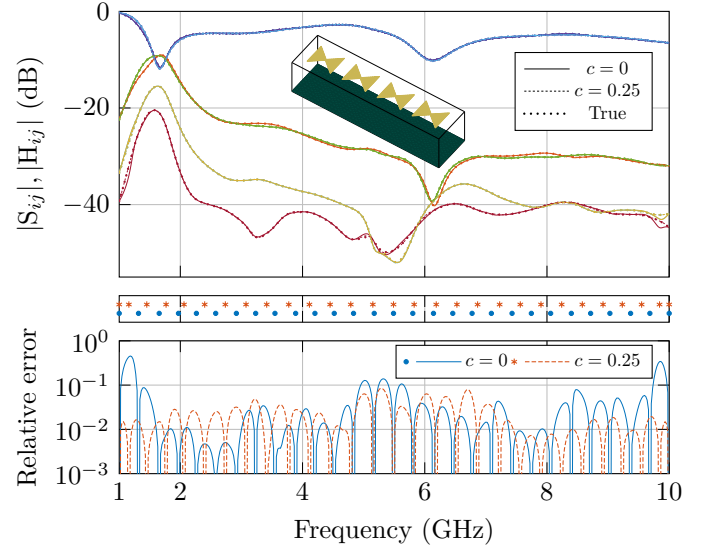


Fig. 4. In the top plot, the true frequency response of the  $4 \times 1$  bowtie array is displayed, as well as the interpolants constructed using 29 interpolation points distributed according to *Cheb* 0 and 0.25. The middle plot shows the corresponding frequency distribution. In the bottom plot, the relative errors of the interpolants are displayed.

Figure 4 displays the interpolated frequency response and the relative error ( $E_{\text{rel}}$  from (19)) obtained from using 29 samples distributed according to *Cheb* 0, *Cheb* 0.25 ( $c = 0, 0.25$ , respectively). Towards the ends of the band of interest, the *Cheb* 0.25 distribution yields a ten times smaller relative error as compared to the equidistant distribution (*Cheb* 0).

#### A. 5G-antenna Example

In this example, we consider the frequency response of a 5G-antenna, see inset in Fig. 6, available in CST microwave studio's component library [31]. The antenna response is calculated for 400 samples in the range 20 GHz to 60 GHz, using CST's MoM solver, depicted in Fig. 6 by the dotted line marked 'True'.

In Fig. 5, the RMSE values obtained for the adaptive sampling methods and the envelope of the minimum of the predetermined distributions are shown. We observe in Fig. 5 that the Loewner framework reaches a consistently lower RMSE compared to vector fitting. The lowest RMSE are achieved by the minimum of the 30 predetermined distributions, and the Theta II adaptive algorithm. None of the adaptive algorithms distinctly outperforms the minimum of the 30 predetermined distributions. The Theta II algorithm does, however, reach similar RMSE values as the minimum of the 30 predetermined distributions, and for some points, the Theta II algorithm even yields a slightly smaller RMSE. Among the adaptive sampling algorithms, Theta II yields a consistently lower RMSE.



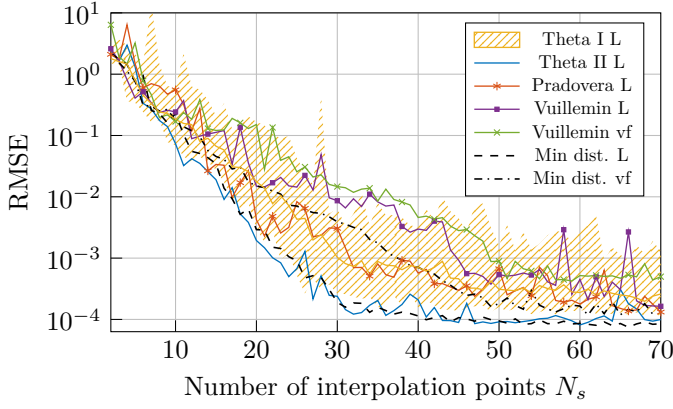


Fig. 5. The RMSE obtained by letting the adaptive and predetermined frequency sampling algorithms use 2 to 70 interpolation points, for the 5G antenna case.

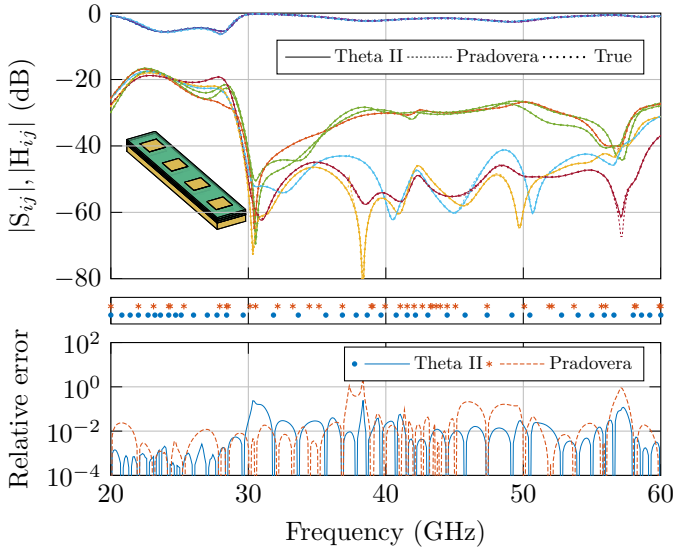


Fig. 6. In the top plot, the true frequency response of the 5G-antenna is displayed, as well as the interpolants constructed using 40 interpolation points sampled according to the Theta II and Pradovera algorithm. The middle plot shows the corresponding frequency distribution. In the bottom plot, the relative errors of the interpolants are displayed.

The surrogate models generated using the Loewner framework yield the results displayed in Fig. 6. For this case, 40 interpolation points have been sampled using the Pradovera and Theta II algorithms, respectively. By sampling according to Theta II, the obtained overall relative error is lower, at most frequencies, than compared to sampling with the Pradovera algorithm, and all other tested adaptive methods. Especially in the regions 20 GHz to 30 GHz (where the mutual coupling is high) 37 GHz to 51 GHz, and 54 GHz to 60 GHz. The obtained sampling distributions using the two adaptive methods differ noticeably. A denser distribution of samples is obtained where the coupling terms are high for the Theta II algorithm.

### B. 7×1-Vivaldi Array

For our next example, the frequency response from a 7 × 1 Vivaldi Array is used, see inset in Fig. 8. The frequency

response is calculated for 400 samples in the range 0.5 GHz to 10 GHz, using an in-house MoM solver, and is illustrated by the dotted line in Fig. 8.

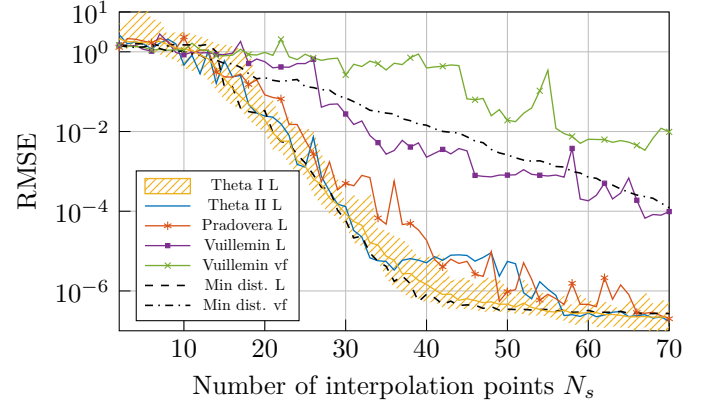


Fig. 7. The RMSE obtained by letting the adaptive and predetermined frequency sampling algorithms use 2 to 70 interpolation points, for the 7 × 1-Vivaldi array.

Figure 7 displays the RMSE from feeding the methods 2 to 70 interpolation points. Observing the yellow and blue lines, the corresponding methods, Theta I and II, yield similar results in terms of RMSE. The two methods perform similarly between 2 to 35 interpolation points. From 35 to 57 interpolation points, the Theta I method yields, on average, a lower RMSE. Up until 35 interpolation points, we also notice that both the Theta I and Theta II algorithms perform as well as the minimum envelope of the 30 predetermined distributions.

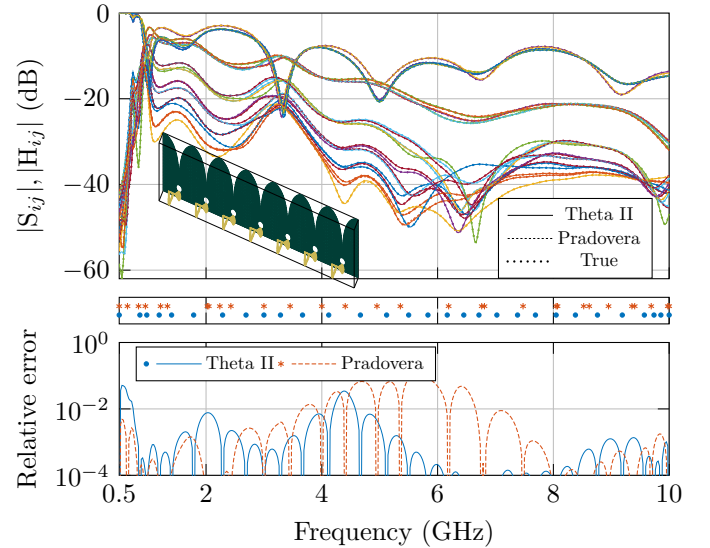


Fig. 8. In the top plot, the true frequency response of the Vivaldi array is displayed, as well as the interpolants constructed using 30 interpolation points sampled according to the Theta II and Pradovera algorithm. The middle plot shows the corresponding frequency distribution. In the bottom plot, the relative errors of the interpolants are displayed.

In Fig. 8, the interpolants generated using the Loewner framework with 30 interpolation points sampled according to the Pradovera algorithm and Theta II are shown. The corresponding relative errors between the true frequency response

and the interpolants are plotted below the sample distribution of the two methods. In the region 4.5 GHz to 8 GHz, there is a significant difference in the relative error between the Theta II and Pradovera algorithms. The Pradovera algorithm samples this region rather sparsely, whereas the Theta II algorithm chooses samples in a more equidistant manner. At the beginning of the frequency band, the Theta II algorithm samples frequency points much sparser than the Pradovera algorithm, leading to a relative error greater than  $10^{-2}$ .

### C. $8 \times 2$ T-Slot Loaded Dipole Array

For the next-to-last benchmarking example, we use the frequency response of a  $8 \times 2$  T-slot loaded dipole array, see inset of Fig. 10. The antenna element used in this example is fully metallic, unlike the original T-slot loaded dipole element from [32]. The frequency response is calculated using an in-house MoM solver for 400 samples in the range 0.5 GHz to 15 GHz, and can be seen in Fig. 10. The frequency band of the simulation has been extended beyond the bandwidth of the antenna to provide rapidly changing out-of-band data to test the methods on.

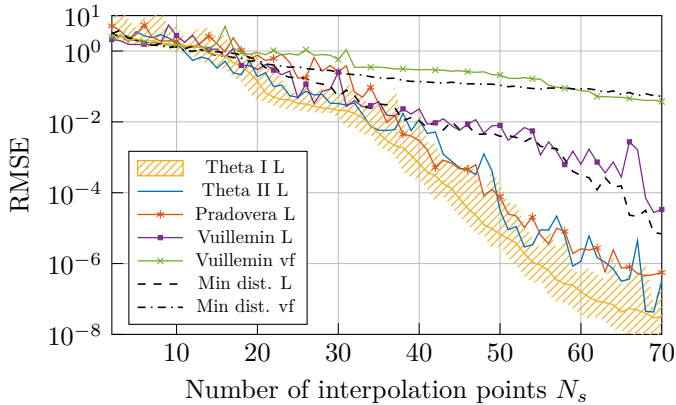


Fig. 9. The RMSE obtained by letting the adaptive and predetermined frequency sampling algorithms use 2 to 70 interpolation points, for the  $8 \times 2$  T-slot loaded dipole array.

In Fig. 9, the RMSE of the sampling methods is displayed. The Theta I algorithm yields a noticeably smaller RMSE for the same number of interpolation points used compared to the other methods. The three adaptive methods, Theta I, Pradovera and Theta II, are observed to yield a distinctly lower RMSE than any predetermined distribution (after 40 interpolation points used). The difference in performance between the Loewner framework and vector fitting is also clear.

Figure 10 shows the interpolants generated from using the Loewner framework with 46 interpolation points sampled according to the Theta I and Pradovera algorithm. In the lower plot of Fig. 10, the relative errors between the interpolants and the true frequency response are displayed. Notice how the Theta I algorithm yields a smooth error distribution around  $10^{-2}$ . Comparing the obtained sampling distributions of the two methods and the frequency response, we see a high distribution of samples in regions with rapid change in the frequency response.

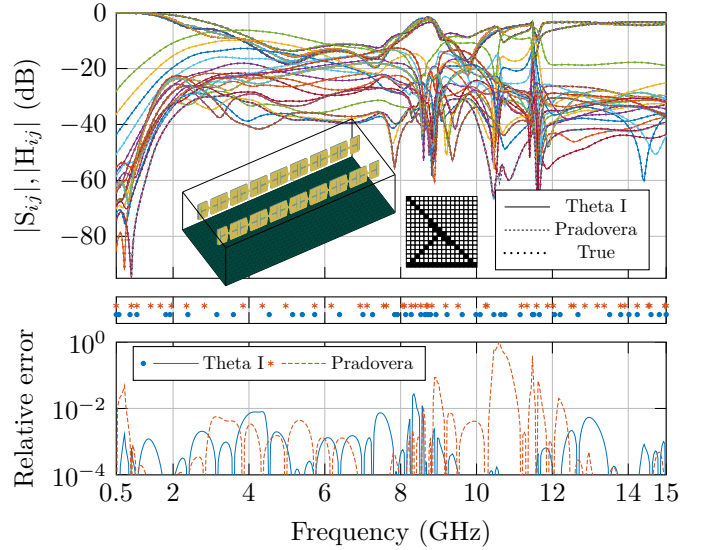


Fig. 10. In the top plot, the true frequency response of the T-slot loaded dipole array is displayed, as well as the interpolants constructed using 46 interpolation points sampled according to the Theta I and Pradovera algorithm. Since the frequency response yields  $16 \times 16$  matrices per frequency, only the elements highlighted by the black squares have been plotted. The middle plot shows the corresponding frequency distribution. In the bottom plot, the relative errors of the interpolants are displayed.

### D. $4 \times 3$ BoR Array

For the last benchmarking example, we use the frequency response of a  $4 \times 3$  BoR array, see inset of Fig. 12, where the BoR element is from [33]. The frequency response is calculated for 300 samples in the range 4 GHz to 20 GHz, using an in-house MoM solver. The frequency response of the BoR array is depicted by the dotted lines in Fig. 12.

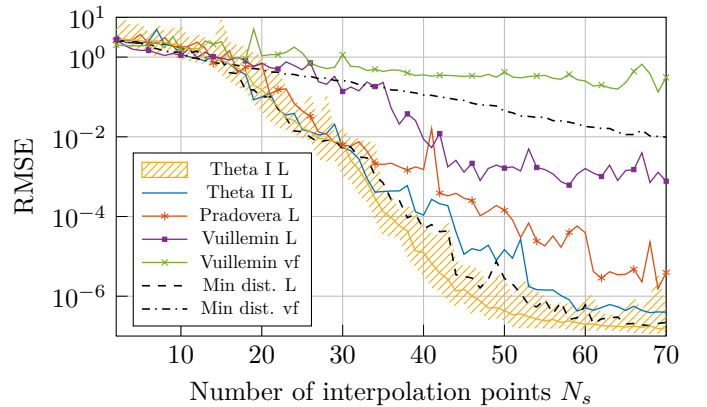


Fig. 11. The RMSE obtained by letting the adaptive and predetermined frequency sampling algorithms use 2 to 70 interpolation points, for the  $4 \times 3$  BoR array.

Figure 11 displays the RMSE of the predetermined and adaptive sampling methods for the BoR array case. Up until 36 interpolation points, the Theta I and II algorithm perform similarly, or better than the minimum of the predetermined distributions. After 37 interpolation points used, the Theta II algorithm yields a slightly higher RMSE than the minimum of the predetermined distributions. The Theta I algorithm,



however, yields a lower RMSE than the minimum of the predetermined distributions.

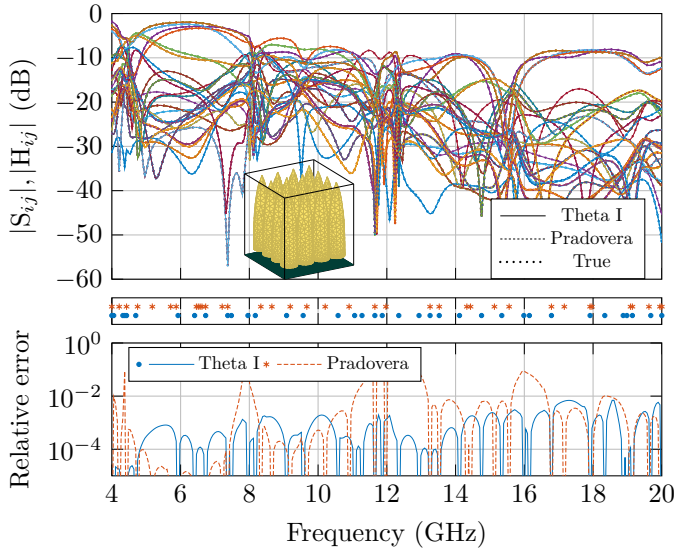


Fig. 12. In the top plot, the true frequency response of the Dipole array is displayed, as well as the interpolants constructed using 37 interpolation points sampled according to the Theta I and Pradovera algorithm. The middle plot shows the corresponding frequency distribution. In the bottom plot, the relative errors of the interpolants are displayed.

In Fig. 12, we display the interpolants constructed using the Loewner framework with 37 interpolation points sampled according to the Theta I and Pradovera algorithm. The lower plot of Fig. 12 displays the corresponding relative error of the interpolants. We observe that the relative error corresponding to the Theta I algorithm is smooth just below  $10^{-2}$ . The relative error corresponding to the Pradovera algorithm is more dynamic in comparison, with regions where the relative error is greater than  $10^{-2}$ .

## V. CONCLUSIONS

We have proposed two novel adaptive frequency sampling algorithms, Theta I, and II, based on the Loewner generating system approach. These adaptive frequency sampling methods are used in conjunction with the Loewner framework and have been compared with other frequency sampling algorithms in four antenna responses. Among the adaptive methods, the Theta II, Theta I, and the Pradovera algorithm succeed in sampling a minimal number of frequency points while still achieving a remarkably low RMSE in the resulting interpolants, demonstrating their performance in maintaining accuracy with reduced computational effort. Additionally, in all of our benchmarking cases, the Loewner framework has shown to provide the most accurate interpolants compared to vector fitting, for all frequency sampling strategies tested in this paper.

Of the three adaptive algorithms, Theta II yields the lowest average RMSE in one of the four antenna cases (the 5G antenna), whereas the Theta I algorithm yields the lowest average RMSE in three of the four antenna cases (The Vivaldi array, the loaded dipole array, and the BoR array).

The proposed Theta I algorithm is appropriate for adaptive sampling for minimizing an error of choice. In this paper, we have used an element-wise relative difference calculation, leading to a minimization of the largest element-wise relative error. The effect of this can be seen by the smoothness of the relative error in the relative error plots of some of the benchmarking cases.

We have also shown that the proposed adaptive sampling algorithms can perform similarly (or better) than the best of the tested predetermined frequency sampling distributions. With the proposed adaptive sampling algorithms together with the Loewner framework, the necessary number of interpolation points can be kept low while still maintaining an accurate interpolant.

## ACKNOWLEDGMENT

This work is supported by project nr ID20-0004 from the Swedish Foundation for Strategic Research and #2022-00833 in the Strategic innovation program Smarter Electronics System – a joint effort by Vinnova, Formas, and Energimyndigheten (Energy Agency), which we gratefully acknowledge.

## REFERENCES

- [1] A. Emadeddin and B. L. G. Jonsson, "A Fully Integrated Filtering Vivaldi Antenna With High Selectivity and Wide Out-of-Band Suppression," *IEEE Access*, vol. 12, pp. 2690–2700, 2024.
- [2] T. Dhaene, J. Ureel, N. Fache, and D. De Zutter, "Adaptive frequency sampling algorithm for fast and accurate S-parameter modeling of general planar structures," in *Proceedings of 1995 IEEE MTT-S International Microwave Symposium*, 1995, pp. 1427–1430 vol.3.
- [3] V. de la Rubia and Z. Peng, "Data-driven model order reduction via Loewner approach for fast frequency sweep in hybrid BI-FEM solution in large finite frequency selective surfaces," in *2017 IEEE MTT-S International Conference on Numerical Electromagnetic and Multiphysics Modeling and Optimization for RF, Microwave, and Terahertz Applications (NEMO)*, 2017, pp. 287–289.
- [4] A. Fenn, G. Thiele, and B. Munk, "Moment method analysis of finite rectangular waveguide phased arrays," *IEEE Transactions on Antennas and Propagation*, vol. 30, no. 4, pp. 554–564, 1982.
- [5] K. Zhao, M. Vouvakis, and J.-F. Lee, "The adaptive cross approximation algorithm for accelerated method of moments computations of EMC problems," *IEEE Transactions on Electromagnetic Compatibility*, vol. 47, no. 4, pp. 763–773, 2005.
- [6] M. Gustafsson, C. Sohl, and G. Kristensson, "Physical limitations on antennas of arbitrary shape," *Proceedings of the Royal Society A: Mathematical, Physical and Engineering Sciences*, vol. 463, no. 2086, pp. 2589–2607, Jul. 2007, publisher: The Royal Society.
- [7] M. Gustafsson and B. L. G. Jonsson, "Antenna Q and Stored Energy Expressed in the Fields, Currents, and Input Impedance," *IEEE Transactions on Antennas and Propagation*, vol. 63, no. 1, pp. 240–249, 2015.
- [8] A. C. Antoulas, *Approximation of Large-Scale Dynamical Systems*. Society for Industrial and Applied Mathematics, 2005.
- [9] C. Beattie and S. Gugercin, "Chapter 7: Model Reduction by Rational Interpolation," in *Model Reduction and Approximation*. Philadelphia, PA: Society for Industrial and Applied Mathematics, 2017, pp. 297–334.
- [10] S. Peik, R. Mansour, and Y. Chow, "Multidimensional Cauchy method and adaptive sampling for an accurate microwave circuit modeling," *IEEE Transactions on Microwave Theory and Techniques*, vol. 46, no. 12, pp. 2364–2371, 1998.
- [11] J. Yang and T. K. Sarkar, "Interpolation/Extrapolation of Radar Cross-Section (RCS) Data in the Frequency Domain Using the Cauchy Method," *IEEE Transactions on Antennas and Propagation*, vol. 55, no. 10, pp. 2844–2851, 2007.
- [12] B. Gustavsen and A. Semlyen, "Rational approximation of frequency domain responses by vector fitting," *IEEE Transactions on Power Delivery*, vol. 14, no. 3, pp. 1052–1061, 1999.

- [13] D. Deschrijver, M. Mrozowski, T. Dhaene, and D. De Zutter, "Macro-modeling of Multiport Systems Using a Fast Implementation of the Vector Fitting Method," *IEEE Microwave and Wireless Components Letters*, vol. 18, no. 6, pp. 383–385, 2008.
- [14] A. C. Antoulas, S. Lefteriu, and A. C. Ionita, "Chapter 8: A Tutorial Introduction to the Loewner Framework for Model Reduction," in *Model Reduction and Approximation*. Philadelphia, PA: Society for Industrial and Applied Mathematics, 2017, pp. 335–376.
- [15] A. J. Mayo and A. C. Antoulas, "A framework for the solution of the generalized realization problem," *Linear Algebra and its Applications*, vol. 425, no. 2, pp. 634–662, 2007.
- [16] D. S. Karachalios, I. V. Gosea, and A. C. Antoulas, "6 The Loewner framework for system identification and reduction," in *Volume 1 System- and Data-Driven Methods and Algorithms*, P. Benner, S. Grivet-Talocia, A. Quarteroni, G. Rozza, W. Schilders, and L. M. Silveira, Eds. Berlin, Boston: De Gruyter, 2021, pp. 181–228.
- [17] Q. Aumann and I. V. Gosea, "Practical challenges in data-driven interpolation: Dealing with noise, enforcing stability, and computing realizations," *International Journal of Adaptive Control and Signal Processing*, vol. n/a, no. n/a, 2023, eprint: <https://onlinelibrary.wiley.com/doi/pdf/10.1002/acs.3691>.
- [18] S. Grivet-Talocia and B. Gustavsen, *Passive Macromodeling*, ser. Wiley Series in Microwave and Optical Engineering. Nashville, TN: John Wiley & Sons, Nov. 2015.
- [19] I. V. Gosea and S. Güttel, "Algorithms for the Rational Approximation of Matrix-Valued Functions," *SIAM Journal on Scientific Computing*, vol. 43, no. 5, pp. A3033–A3054, Jan. 2021, publisher: Society for Industrial and Applied Mathematics.
- [20] B. Salarieh and H. M. J. D. Silva, "Review and comparison of frequency-domain curve-fitting techniques: Vector fitting, frequency-partitioning fitting, matrix pencil method and loewner matrix," *Electric Power Systems Research*, vol. 196, p. 107254, 2021.
- [21] S. Lefteriu and A. C. Antoulas, "A New Approach to Modeling Multiport Systems From Frequency-Domain Data," *IEEE Transactions on Computer-Aided Design of Integrated Circuits and Systems*, vol. 29, no. 1, pp. 14–27, 2010.
- [22] J. Becerra, Z. López, A. Rangel, and F. Vega, "A Comparison of Fitting Methods for Modeling the Front Door Coupling of Two Nearby Parabolic Antennas," in *2018 USNC-URSI Radio Science Meeting (Joint with AP-S Symposium)*, 2018, pp. 27–28.
- [23] M. Gustafsson, L. Jelinek, K. Schab, and M. Capek, "Unified Theory of Characteristic Modes—Part II: Tracking, Losses, and FEM Evaluation," *IEEE Transactions on Antennas and Propagation*, vol. 70, no. 12, pp. 11 814–11 824, 2022.
- [24] H.-B. Yuan, W.-T. Bao, C. H. Lee, B. F. Zinser, S. Campione, and J.-F. Lee, "A Method of Moments Wide Band Adaptive Rational Interpolation Method for High-Quality Factor Resonant Cavities," *IEEE Transactions on Antennas and Propagation*, vol. 70, no. 5, pp. 3595–3604, 2022.
- [25] H. Yuan, J. Ren, Y. Li, and L. Su, "Removing the Froissart Doublets in a Rational Interpolation for S-parameters," in *2022 IEEE 10th Asia-Pacific Conference on Antennas and Propagation (APCAP)*, 2022, pp. 1–2.
- [26] B. L. G. Jonsson, "Model Order Reduction for Parametric Dependence of Q-factor Bounds in IoT Applications," in *2024 18th European Conference on Antennas and Propagation (EuCAP)*, 2024, pp. 1–4.
- [27] D. Pradovera, "Toward a certified greedy Loewner framework with minimal sampling," *Adv. Comput. Math.*, vol. 49, no. 6, Dec. 2023, place: Berlin, Heidelberg Publisher: Springer-Verlag.
- [28] P. Vuillemin and C. Poussot-Vassal, "Constructive interpolation points selection in the Loewner framework," Aug. 2021, arXiv:2108.13042 [cs, eess, math].
- [29] K. Cherifi, P. Goyal, and P. Benner, "A greedy data collection scheme for linear dynamical systems," *Data-Centric Engineering*, vol. 3, p. e16, 2022.
- [30] J. Yang and T. K. Sarkar, "Accurate Interpolation of Amplitude-Only Frequency Domain Response Based on an Adaptive Cauchy Method," *IEEE Transactions on Antennas and Propagation*, vol. 64, no. 3, pp. 1005–1013, 2016.
- [31] Dassault Systèmes, "Cst studio suite." [Online]. Available: <https://www.3ds.com/products/simulia/cst-studio-suite>
- [32] C. I. Kolitsidas and B. L. G. Jonsson, "Rectangular vs. equilateral triangular lattice comparison in a T-slot loaded strongly coupled dipole array," in *2014 XXXIth URSI General Assembly and Scientific Symposium (URSI GASS)*, 2014, pp. 1–4.
- [33] H. Holter, "Dual-Polarized Broadband Array Antenna With BOR-Elements, Mechanical Design and Measurements," *IEEE Transactions on Antennas and Propagation*, vol. 55, no. 2, pp. 305–312, 2007.